

Modeling surface motion effects in N₂ dissociation on W(110): *Ab initio* molecular dynamics calculations and generalized Langevin oscillator model

Cite as: J. Chem. Phys. **144**, 244708 (2016); <https://doi.org/10.1063/1.4954773>

Submitted: 11 April 2016 . Accepted: 13 June 2016 . Published Online: 29 June 2016

Francesco Nattino, Oihana Galparsoro, Francesca Costanzo, Ricardo Díez Muiño, Maite Alducin, and Geert-Jan Kroes 



View Online



Export Citation



CrossMark

ARTICLES YOU MAY BE INTERESTED IN

[N₂ dissociation on W\(110\): An *ab initio* molecular dynamics study on the effect of phonons](#)

The Journal of Chemical Physics **142**, 104702 (2015); <https://doi.org/10.1063/1.4913979>

[Electron-hole pair effects in methane dissociative chemisorption on Ni\(111\)](#)

The Journal of Chemical Physics **145**, 044704 (2016); <https://doi.org/10.1063/1.4959288>

[Dynamics of H₂ dissociation on the close-packed \(111\) surface of the noblest metal: H₂ + Au\(111\)](#)

The Journal of Chemical Physics **145**, 144701 (2016); <https://doi.org/10.1063/1.4964486>

The Journal
of Chemical Physics

2018 EDITORS' CHOICE

READ NOW!



Modeling surface motion effects in N₂ dissociation on W(110): *Ab initio* molecular dynamics calculations and generalized Langevin oscillator model

Francesco Nattino,^{1,a)} Oihana Galparsoro,^{2,3,4,a)} Francesca Costanzo,^{1,b)}

Ricardo Díez Muiño,^{2,5} Maite Alducin,^{2,5} and Geert-Jan Kroes¹

¹*Leiden Institute of Chemistry, Leiden University, Gorlaeus Laboratories, P.O. Box 9502, 2300 RA Leiden, The Netherlands*

²*Donostia International Physics Center (DIPC), Paseo Manuel de Lardizabal 4, 20018 Donostia-San Sebastián, Spain*

³*Université de Bordeaux, F-33400 Talence, France*

⁴*CNRS, ISM, UMR 5255, F-33400 Talence, France*

⁵*Centro de Física de Materiales CFM/MPC (CSIC-UPV/EHU), Paseo Manuel de Lardizabal 5, 20018 Donostia-San Sebastián, Spain*

(Received 11 April 2016; accepted 13 June 2016; published online 29 June 2016)

Accurately modeling surface temperature and surface motion effects is necessary to study molecule-surface reactions in which the energy dissipation to surface phonons can largely affect the observables of interest. We present here a critical comparison of two methods that allow to model such effects, namely, the *ab initio* molecular dynamics (AIMD) method and the generalized Langevin oscillator (GLO) model, using the dissociation of N₂ on W(110) as a benchmark. AIMD is highly accurate as the surface atoms are explicitly part of the dynamics, but this advantage comes with a large computational cost. The GLO model is much more computationally convenient, but accounts for lattice motion effects in a very approximate way. Results show that, despite its simplicity, the GLO model is able to capture the physics of the system to a large extent, returning dissociation probabilities which are in better agreement with AIMD than static-surface results. Furthermore, the GLO model and the AIMD method predict very similar energy transfer to the lattice degrees of freedom in the non-reactive events, and similar dissociation dynamics. *Published by AIP Publishing.* [<http://dx.doi.org/10.1063/1.4954773>]

I. INTRODUCTION

The dissociation of diatomic molecules on metal surfaces represents the simplest class of molecule-metal surface reactions. The simplicity, however, is only apparent, as theory still struggles to achieve quantitative agreement with experiment on dynamical observables such as the dissociation probability for various molecule-surface systems.¹

One of the approximations on which state-of-the-art calculations often rely and which is often blamed for such discrepancies is the ideal and static surface approximation, which assumes the metal atoms to remain fixed at their equilibrium position during the whole course of the dynamics. This approximation enormously simplifies the complexity of the problem, reducing the dimensionality of the molecule-surface interaction potential to the six molecular degrees of freedom. In fact, a six dimensional potential energy surface (PES) can be pre-computed for some selected nuclear configurations, accurately interpolated and readily employed to perform dynamics. However, the ideal and static surface approximation neglects the effects that (i) the thermal displacement of the surface atoms from their equilibrium positions (*surface temperature* effects), which could be due to

the thermal motion of the surface atoms or to the lattice thermal expansion, and (ii) the energy exchange between the molecule and the lattice (*surface motion* or *recoil* effects) might have on a given gas-surface reaction.^{2,3} The first type of effects is expected to be important, for instance, when considering an activated dissociative chemisorption process the barrier height of which is strongly affected by the displacement of the surface atoms.^{4,5} The second class of effects is expected to be more relevant whenever the ratio between the mass of the molecule and the mass of the surface atoms is close to one. Under such condition, in fact, the energy transfer to the lattice is most efficient^{6–8} and could translate into less energy being available to the molecule to overcome eventual dissociation or desorption barriers.

In the past years, significant work has been directed at including surface temperature and surface motion effects in more realistic dynamical models. One of such models is the generalized Langevin oscillator (GLO) model,^{9–13} in which the surface is effectively represented as a harmonic oscillator (surface oscillator, SO) as in the SO model.¹⁴ This first oscillator is then coupled to a second harmonic oscillator (ghost oscillator) which accounts for the energy transferred to the lattice through a dissipative term. Within this model, the molecule-surface interaction potential is still represented with a pre-calculated six dimensional (6D) PES that accounts only for the molecular degrees of freedom,

^{a)}F. Nattino and O. Galparsoro contributed equally to this work.

^{b)}Present address: Catalan Institute of Nanoscience and Nanotechnology, Campus de la UAB, Edifici ICN2 08193 Bellaterra, Spain.

which makes this model computationally convenient. The GLO model has been applied to various molecule-surface systems^{12,13,15–20} and, in spite of its simplicity, it has provided improved agreement with experimental data compared to the corresponding ideal and static surface models. These findings suggested that the GLO model was able to capture the physics of the systems investigated, at least for the observables of interest.

With the growth of computational power and the development of efficient algorithms, the use of *ab initio* molecular dynamics (AIMD) to estimate the dissociation probability for molecules on metal surfaces with reasonable statistical accuracy has recently become possible.^{21–24} In AIMD, the forces acting on the nuclei are calculated on-the-fly, and this allows to accurately account for the effect of surface atom displacements and of surface temperature and lattice recoil, through the modeling of surface atom motion. However, the need of performing an electronic structure calculation at each time step makes the AIMD technique orders of magnitude more computationally demanding than PES-based approaches, and the lowest reaction probabilities (<1%) are, therefore, at present out of the reach of this technique.

Here, we perform a critical comparison of the AIMD method and the GLO model in the study of a molecule-surface reaction that was recently shown to be strongly affected by surface motion effects,²⁴ namely, the dissociation of N₂ on W(110). Our aim is to validate the GLO model against the more accurate, but more computationally expensive, AIMD method, and to investigate to which extent the GLO model can be employed to accurately model the considered dissociation reaction. The dissociation of nitrogen on metals is relevant as a model system for heterogeneous catalysis, as the N₂ dissociative adsorption on an iron catalyst is believed to be the rate limiting step of the industrial ammonia synthesis (Haber-Bosch) process.²⁵ However, in spite of the large number of experimental^{26–33} and theoretical^{24,34–48} studies that investigated this reaction, an accurate description of the dissociative chemisorption of nitrogen on tungsten surfaces is still lacking.¹ Two dissociation channels have been found for this system.^{24,38,41,47} Molecules can dissociate upon their first approach to the surface, in what has been called a *direct* dissociation mechanism, or through more complicated paths that are accompanied by multiple rebounds on the surface (*indirect* or *trapping-mediated* mechanism). In particular this last mechanism is strongly affected by the modeling of surface atom motion, as the dissipation of energy to surface phonons can largely increase the probability for the impinging molecules to be trapped on the surface, thereby increasing their chance to react.^{24,48} In N₂ + W(110), the molecular trapping is facilitated by the availability of various molecular chemisorption wells, which, depending on the density functional used, theory predicts to be as deep as −1.4 eV.²⁴

We have found that the GLO model and the AIMD method qualitatively agree in how surface motion and surface temperature effects affect the dissociation probability of N₂ on W(110). Both methods, in fact, suggest the energy transfer to phonons to increase the reactivity of

this system through enhanced trapping-mediated dissociation, compared to static-surface data. The GLO model and the AIMD method also generally agree in predicting the energy that scattering molecules transfer to the surface and in the comparison of a few features of the dissociation dynamics.

The structure of this article is as follows. The AIMD method and the GLO model are presented in Section II. In Section III, the results are presented and discussed. In particular, the AIMD method and the GLO model are compared for the dissociation probabilities (Section III A), some features of the dissociation dynamics (Section III B) and the energy transferred to the surface phonons (Section III C). The comparison of both AIMD and GLO dissociation probabilities to experimental data is then presented in Section III D. Finally, the conclusions are presented in Section IV.

II. METHODS

Both the AIMD method and the GLO model rely on the Born-Oppenheimer approximation, according to which the dynamics of the nuclei is assumed to take place on the instantaneous electronic ground state, therefore neglecting electron-hole pair excitations.

Density functional theory (DFT) at the generalized gradient approximation (GGA) level has been employed for the electronic structure calculations. Previous work^{41,46} has highlighted the strong effect that the choice of the exchange-correlation functional can have on the reactive and the non-reactive scattering of N₂ from W(110). For this reason, two PESs, based on the PW91^{49,50} and on the RPBE⁵¹ density functionals, respectively, have been employed in combination with the GLO model, and the PBE^{52,53} and the RPBE functionals have been used in the AIMD method. Density functionals that approximately account for the van der Waals interaction^{54–56} have been shown^{47,48} to improve adsorption energies as well as dissociation and desorption barriers with respect to available energetics from temperature programmed desorption and electron stimulated desorption experiments.^{30,31} These van der Waals-corrected functionals have also been shown^{47,48} to improve, to a certain extent, the agreement with experimental dissociation probabilities.^{29,32} However, considering that our purpose here is merely to compare the GLO model to the AIMD method, traditional semi-local functionals like PW91/PBE and RPBE have been employed in the present study.

Details on the two PESs,^{37,38,41} on the AIMD methodology,²⁴ and on the GLO model employed¹⁵ have been given previously, therefore we will be brief here. A 2 × 2-supercell 5-layer slab has been employed to model the metal surface. The same plane-wave DFT code VASP^{57–61} and very similar computational setups have been employed in the electronic structure calculations in both the preparation of the PESs and in the AIMD calculations (see also Ref. 24). Note that the well-known similarity⁵² between the PBE and the PW91 energetics allows one to compare GLO results obtained with the PW91-PES to results from PBE-AIMD calculations, in a similar way as results obtained from GLO calculations with

the RPBE-PES can be compared to results from RPBE-AIMD calculations.

In order to obtain a continuous representation of each 6D PES the corrugation reducing procedure⁶² was used to interpolate a set of 5610 DFT energy points that were calculated for different configurations of N_2 over an ideal W(110) surface. The same set of configurations was used to build the PW91 and the RPBE energy grids. The accuracy of the two interpolated PESs is rather satisfactory, except for errors of about 100 meV that can be found for some orientations of the molecule when it is located close to the surface ($Z \lesssim 2.5$ Å). However, the effect of such errors on the dissociation probability is noticeable only at normal incidence for energies below 0.5 eV.⁴⁷ These interpolation errors are not expected to be relevant for the purpose of the present study, that is, the comparison between the GLO model and the AIMD method in describing surface temperature effects and energy transfer to the lattice, at the incidence conditions considered here.

In order to model surface temperature effects in AIMD, the initial conditions of the surface atoms randomly sample the position and the velocities assumed in one out of ten differently initialized clean surface dynamical runs. Furthermore, the equilibrium lattice constant of tungsten has been expanded according to experimental information⁶³ in order to account for the (rather small) thermal expansion of the lattice (0.37% at 800 K). The root mean square displacement (RMSD) calculated for the surface atoms in the clean surface dynamical runs has been found²⁴ to agree well with the RMSD value calculated for similar dynamical runs performed simulating a 3×3 surface unit cell (for the PBE functional only), suggesting that the 2×2 cell employed is sufficiently large for properly sampling the initial displacements of the surface atoms at the simulated temperature (800 K).

In the GLO calculations, the W(110) surface motion is described in terms of a three-dimensional (3D) harmonic oscillator with the mass of one W atom (surface oscillator). Coupled to it, a second 3D oscillator of identical mass (ghost oscillator), which is subjected to a friction and a random force, acts as the thermal bath provided by the bulk. The friction and random forces are related through the second fluctuation-dissipation theorem to specifically account for energy dissipation and thermal fluctuations. The frequencies associated with both oscillators for the parallel (ω_x and ω_y) and perpendicular motion (ω_z) are represented by the surface phonon frequencies close to the edges of the W(110) surface Brillouin zone. In particular, we take $\omega_x = \omega_y = 19$ meV and $\omega_z = 16$ meV.⁶⁴ Following Ref. 10, the friction coefficient of the ghost oscillator is obtained from the Debye frequency. Note that neither the dissociation probability nor the energy exchanged with the lattice seems very sensitive to the exact value of these parameters, as long as they are kept within the same order of magnitude (see Figures S1 and S2 in the [supplementary material](#)).

In the GLO method, the PES describing the interaction of the molecule with the surface is taken the same as in the static surface calculations, except that the center of mass coordinates of the molecule are replaced by new coordinates, in which the coordinates of the surface oscillator are subtracted from the

molecule's center of mass coordinates. The GLO method is therefore able to describe the effect of the nearest surface atom on the molecule-surface interaction in an approximate way. However, it can describe neither the effects of surface atoms that are further away nor collective relaxation effects of the surface.

In both AIMD and GLO calculations, the quasi-classical trajectory (QCT) method has been implemented, meaning that the vibrational zero-point energy (ZPE) of N_2 has been initially imparted to the simulated molecules. The surface temperature that we have modeled, $T_S = 800$ K, corresponds to the temperature at which the available sticking experiments^{29,32} have been performed for $N_2 + W(110)$. The dissociative chemisorption at two (polar) incidence angles ($\Theta_i = 0^\circ$, or normal incidence, and $\Theta_i = 60^\circ$) has been simulated, and in the absence of pertinent experimental information a random azimuthal angle of approach has been chosen for the molecules impinging on the surface at off-normal incidence. AIMD (GLO) reaction probabilities have been estimated through the computation of 400 (10 000) trajectories per functional, collision energy, and incidence angle. As a measure of the statistical error associated with the AIMD reaction probabilities we report error bars corresponding to 68% confidence intervals calculated as the normal approximation (or Wald) intervals.⁶⁵

Following a definition employed in previous work,^{38,39,41} we consider a molecule as trapped if it performs at least four rebounds on the surface, i.e., if the center of mass velocity changes from being directed towards the surface to being directed away from the surface for four times. Note that this operational definition is slightly different from the definition employed in Ref. 24, as a rebound was defined as a two-times change of the sign of the molecule's center of mass velocity in the direction perpendicular to the surface, leading to minor differences in the quantification of the direct and the indirect reaction probabilities. Note also that the arbitrariness in the choice of the number of rebounds that define a trapping event does not influence our conclusions, as it is only used here to describe trends and to compare theoretical models.

The maximum propagation time of the molecule-surface dynamics is 25 ps for the GLO model, but only 2.7 ps for AIMD (extended to 4 ps for the lowest collision energies, where the trapping probability is the largest), due to the high computational cost of this technique. The molecules which are still trapped at the end of the maximum propagation time without dissociating could be quite arbitrarily considered as molecularly chemisorbed. Considering the different maximum propagation times employed in GLO and AIMD and in order to make the methods better comparable, we rather employ the fraction of trapped but non-dissociated molecules to define an upper-bound to the dissociation probability, calculated assuming that all these trapped molecules would dissociate upon further propagation.

The coordinate system employed is sketched in Figure 1, where we have also indicated the molecular degrees of freedom considered as well as some of the most relevant high symmetry impact sites on the surface.

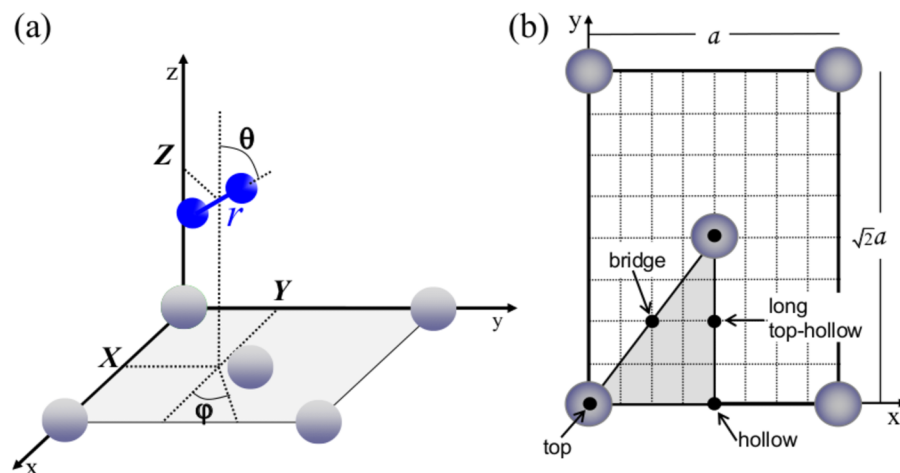


FIG. 1. The coordinate system employed is sketched in panel (a). The relevant high symmetry impact sites on the surface are indicated in panel (b).

III. RESULTS AND DISCUSSION

A. Dissociation probability

The first observable that we consider in the comparison of the GLO model to the AIMD method is the dissociation probability. In Figure 2, AIMD and GLO dissociation probabilities are plotted as a function of the collision energy E_i and compared to the dissociation probabilities calculated with the QCT method on the PW91- and RPBE-PESs but neglecting the action of the surface oscillators, making use of the static surface approximation as in Refs. 37, 38, and 41. Note that the initial vibrational ZPE was not imparted to the simulated molecules in Refs. 37 and 41, while in the present work all static surface and GLO calculations employed the QCT method. We also report two reaction

probabilities calculated with AIMD simulating a static and ideal surface (PBE, normal incidence and $E_i = 1.3$ eV²⁴ and RPBE, $\Theta_i = 60^\circ$ and $E_i \approx 2.3$ eV). These points are in relatively good agreement with the static surface data calculated from the interpolated PESs. Furthermore, a similar level of agreement was found⁴⁷ between static-surface AIMD calculations and calculations performed on the PW91- and the RPBE-PES, at least for the incidence conditions for which we report AIMD data here. These findings suggest that the (computationally cheaper) PES-based results can be employed as a static surface reference to assess the effect of surface temperature in both AIMD and GLO calculations.

At normal incidence, AIMD and GLO reaction probabilities are generally larger than static surface reaction

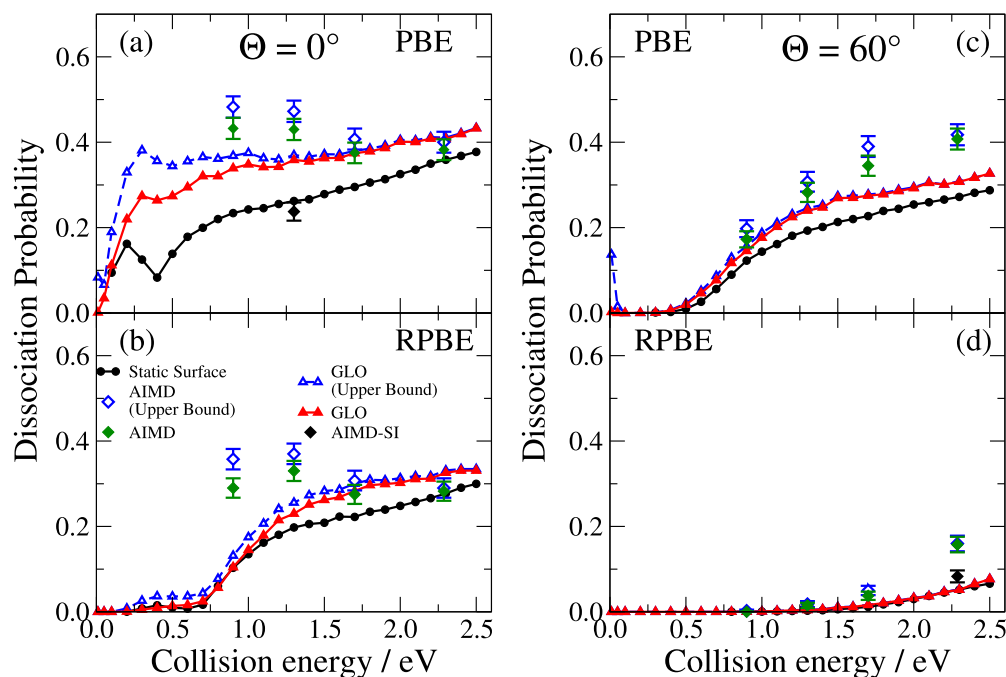


FIG. 2. Dissociation probabilities as a function of the collision energy from PES-based static-surface (black circles) and GLO calculations (red triangles), and from AIMD calculations (green diamonds). Dissociation probabilities calculated simulating a static and ideal surface with AIMD are also plotted as black diamonds for two combinations of incidence conditions and functional used. The QCT method has been employed in all models. Panels (a) and (b) are for normal incidence, and panels (c) and (d) for $\Theta_i = 60^\circ$. Panels (a) and (c) compare PBE-AIMD results to PW91 GLO and static surface results, and panels (b) and (d) compare results obtained with RPBE. Upper bounds to dissociation probabilities calculated assuming the molecular trapping as a contribution to the dissociation probability are plotted using empty blue symbols.

probabilities and in good agreement with each other, apart from the lowest collision energies simulated with AIMD, $E_i = 0.9$ and 1.3 eV. At these collision energies, the difference between the AIMD and the static surface reaction probabilities is also the largest, as already discussed in Ref. 24. The GLO model returns dissociation probabilities that differ most from the static surface probabilities at $E_i \approx 0.4$ eV if the PW91-PES is employed, but at a larger collision energy ($E_i \approx 1.75$ eV) if the RPBE-PES is employed.

Also for $\Theta_i = 60^\circ$ both the AIMD method and the GLO model predict larger dissociation probabilities than the static-surface model. For AIMD, the largest deviations from static surface calculations are observed at the highest collision energy simulated ($E_i \approx 2.3$ eV), independently from whether the PBE functional or the RPBE functional is considered. The GLO probabilities are most different from static surface probabilities at $E_i \approx 1.5$ eV for the calculations on the PW91-PES, while no significant deviations between the two dynamical models are observed when the RPBE functional is considered. The agreement between AIMD and GLO is good at low collision energies, but it becomes worse with increasing E_i . Overall, the agreement between the AIMD dissociation probabilities and the dissociation probabilities computed on the pre-calculated PESs improves when surface temperature effects are modeled through the GLO model.

The upper bounds to dissociation probabilities, calculated assuming that all the molecules that are trapped in the proximity of the surface at the end of the propagation time will eventually dissociate, are also plotted in Figure 2 for AIMD and GLO. The GLO model predicts the largest molecular adsorption probability for the PW91-PES at normal incidence for $0.2 \text{ eV} < E_i < 0.3 \text{ eV}$, making the difference between

the dissociation probabilities and their corresponding upper bounds the highest. We note in passing that with the PW91-PES, GLO calculations predict a finite molecular trapping probability at vanishing collision energies, as the upper bound for the dissociation probability at very low E_i is about 10%, while the dissociation probability at the same collision energy is $\approx 10^{-3}$. This is consistent with the availability of barrierless paths above the top site^{37,38,41} that allow molecules to access local minima of the potential where they can dissipate the (small) initial kinetic energy available. The comparison between AIMD and GLO dissociation probabilities is not much affected by the use of the upper bounds to dissociation probabilities in place of the actual dissociation probabilities.

In Ref. 24 we have already discussed the cause of the increased reactivity observed when modeling surface motion effects with AIMD, comparing the dissociation probabilities calculated at normal incidence to the dissociation probabilities obtained through the ideal and static surface approximation. The observed increases in reactivity were found to be due to a dramatic increase in the indirect component of the dissociation probability, and we suggested that this is due to the impinging molecules being more easily stabilized on the surface through the energy dissipation to the lattice degrees of freedom, increasing their chance to dissociate.

The same argument is expected to apply to the comparison of the GLO dissociation probabilities to the static-surface dissociation probabilities, as the GLO model accounts for the possibility of energy loss to surface phonons. Indeed, when looking at the direct and indirect components of the dissociation probability plotted as a function of incidence energy in Figure 3, we observe a strong increase in the indirect reactivity when going from the static-surface to the GLO

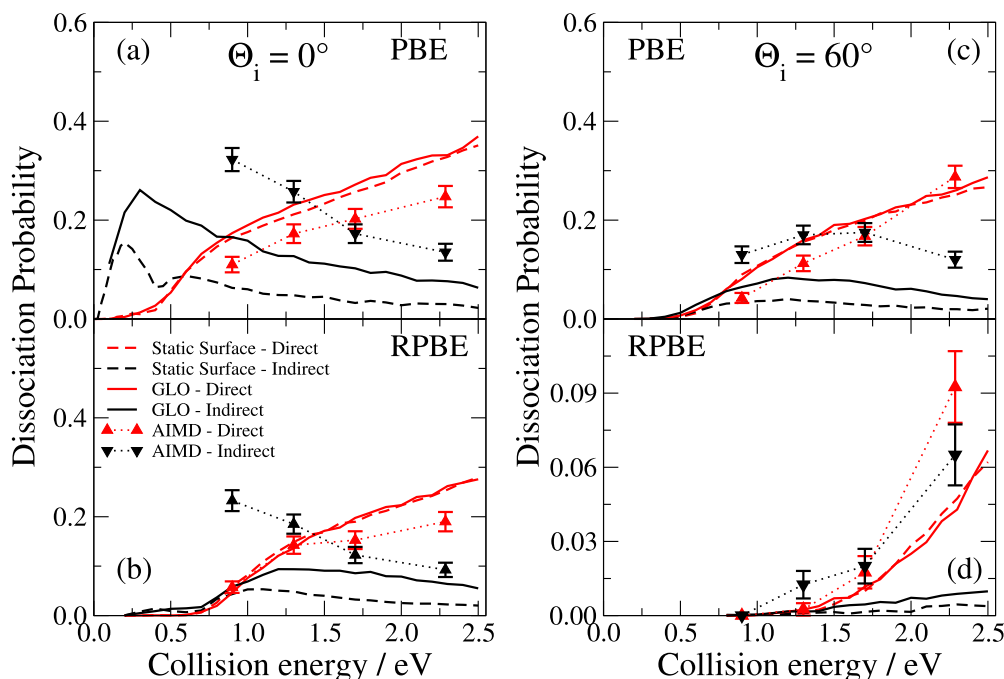


FIG. 3. The direct and indirect contributions to the dissociation probability are plotted for all the theoretical methods as a function of the collision energy in red and black, respectively: dashed lines are for static-surface calculations, solid lines are for GLO, and triangles are for AIMD. The QCT method has been employed in all models. Panels (a) and (b) are for normal incidence and (c) and (d) are for $\Theta_i = 60^\circ$. Panels (a) and (c) are for PBE (apart from static surface and GLO results which are for PW91) and (b) and (d) are for RPBE. Note that the y axis in the (d) panel is plotted on a different scale compared to the other panels, to better show the difference between the various curves.

model. This is true for both PESs and incidence angles, with exception of the RPBE calculations at $\Theta_i = 60^\circ$, where static surface and GLO indirect dissociation probabilities are almost identical. The direct dissociation channel remains almost unaffected by the modeling of surface motion effects through the GLO for all functionals, incidence angles, and collision energies. As already observed for the normal incidence case,²⁴ also for $\Theta_i = 60^\circ$ the AIMD indirect dissociation probabilities are considerably larger than the static surface ones, while direct dissociation probabilities are generally closer to each other (Figure 3).

Figure 3 also shows that the discrepancies observed between the AIMD and GLO (total) dissociation probabilities (Figure 2) are mainly due to differences for the indirect channel, with the GLO model underestimating the trapping-mediated reactivity as predicted by the AIMD method. Nevertheless, as for the total dissociation probabilities, also for the indirect dissociation probabilities the agreement with the AIMD data is improved when going from the static surface to the GLO model.

In order to understand the discrepancy between AIMD and GLO reaction probabilities, we now consider the trapping probability, defined as the probability for an incoming molecule to perform more than four rebounds on the surface (see Section II for the definition of rebound), as predicted by the two models. Figure 4 shows GLO and AIMD trapping probabilities as a function of the initial collision energy. For both PBE-AIMD and PW91-GLO calculations, the trapping probability first increases, then decreases with increasing collision energy, with the position of the maximum occurring

at higher values of E_i for $\Theta_i = 60^\circ$ than for normal incidence. The presence of a maximum in the trapping probability curve can be explained as follows. At low collision energy, only few molecules can access the area close to the surface where they can become trapped. Increasing the collision energy first increases the number of molecules that are able to access this area of the PES, thereby increasing the trapping probability. Increasing the collision energy even further, however, causes a decrease in the trapping probability because the fraction of molecules dissociating through a direct mechanism starts to rise and, at the same time, it becomes more difficult for a molecule to be stabilized in an adsorption state.

For the PW91 (PBE) calculations, the shape of the trapping probability curves resembles the shape of the trapping-mediated dissociation probability curves for both incidence angles (Figure 3). This is consistent with previous observations according to which the trapping-mediated dissociation probability is a function of the trapping probability, while the dissociation probability of the trapped molecules does not depend on the initial collision energy.²⁴ For what concerns the AIMD/GLO comparison, the trapping-mediated dissociation probability curves as calculated with the PBE (or PW91) functional are qualitatively similar, when considering the same incidence angle. The fact that the PBE-AIMD trapping-mediated reactivity is quantitatively larger than the PW91-GLO one can be explained on the basis of the larger trapping probability obtained with the first method, as expected if surface relaxation effects are present, as they can stabilize a molecule in an adsorption state. In fact, allowing the surface atoms of the first two layers to relax for the three

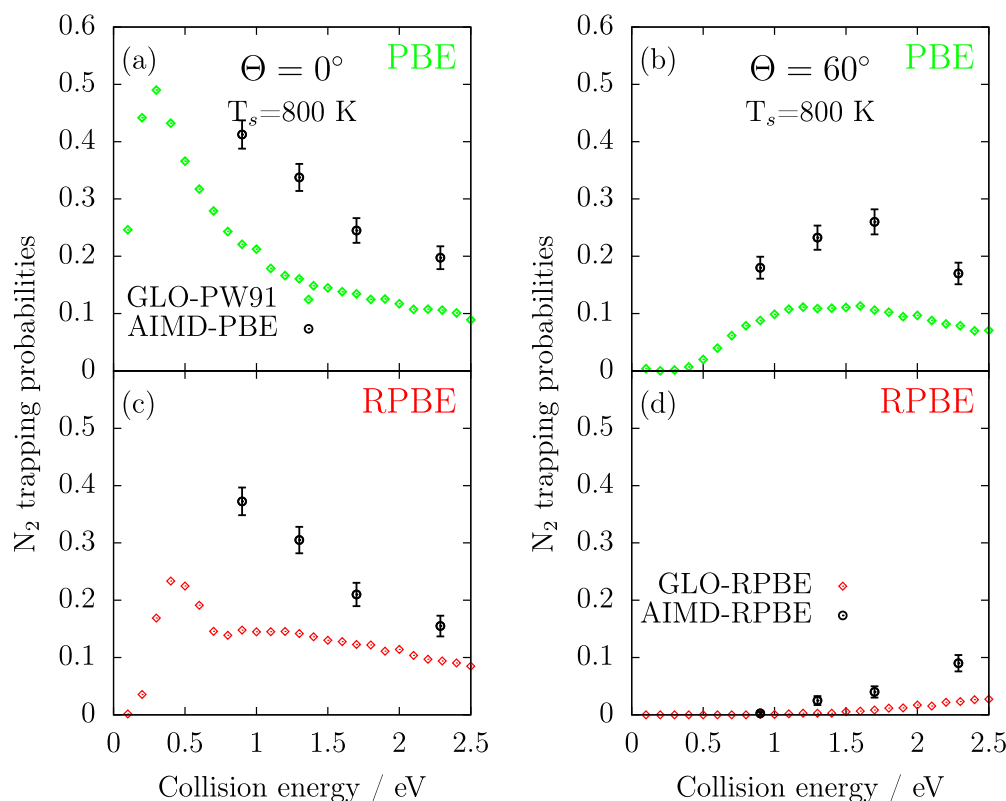


FIG. 4. N_2 trapping probabilities as a function of incidence energy (AIMD results as circles, GLO results as diamonds): (a) PBE (PW91 for GLO) and normal incidence, (b) PBE (PW91 for GLO) and 60° incidence, (c) RPBE and normal incidence, and (d) RPBE and 60° incidence.

TABLE I. Direct, indirect, and total dissociation probabilities calculated with various dynamical methods at $E_i \approx 2.3$ eV and $\Theta_i = 60^\circ$ using the RPBE density functional. The QCT method has been employed in all models. The upper bounds to the dissociation probability are calculated assuming that all the molecules that are trapped at the end of the propagation time will dissociate.

RPBE, $E_i \approx 2.3$ eV, $\Theta_i = 60^\circ$	S_{direct}	$S_{indirect}$	S_{total}	$S_{upper\ bound}$
RPBE-PES—static surface	0.047	0.005	0.052	0.052
RPBE-PES—GLO	0.043	0.009	0.052	0.052
AIMD—static surface, ideal	0.083 ± 0.014	0.000 ± 0.001	0.083 ± 0.014	0.083 ± 0.014
AIMD—static surface, distorted	0.080 ± 0.014	0.008 ± 0.004	0.088 ± 0.014	0.088 ± 0.014
AIMD—moving surface, ideal	0.085 ± 0.014	0.045 ± 0.010	0.130 ± 0.017	0.153 ± 0.018
AIMD—moving surface, distorted	0.093 ± 0.014	0.065 ± 0.012	0.158 ± 0.018	0.160 ± 0.018

molecular adsorption minima reported in Ref. 24 stabilizes the top-vertical and the hollow-parallel adsorption states by about 0.1 eV, and the bridge/hollow-tilted adsorption state by about 0.2 eV, for both the PBE and the RPBE functionals.

The situation is partially different if the RPBE functional is considered. In the RPBE-PES, the difference between the barriers for desorption and for dissociation is significantly smaller than in the PW91-PES.⁴¹ For normal incidence, at collision energies between 0.25 eV and 0.75 eV, significant trapping occurs with the GLO model (Figure 4), but the trapping-mediated dissociation at the same collision energies is close to zero (Figure 3). Only for $E_i > 0.75$ eV, when also the direct dissociation starts to occur, the trapping-mediated reaction curve rises. Almost all the molecules that are trapped for $E_i < 0.75$ eV are instead scattered back towards the vacuum and the inclusion of energy dissipation to the lattice

degrees of freedom through the GLO model does not help to increase the trapping-mediated dissociation. For $\Theta_i = 60^\circ$, the repulsive character of the RPBE-PES at large distances from the surface limits the number of molecules that can approach the surface and become trapped. Even at the highest collision energies simulated no difference is observed between the GLO and the static-surface indirect dissociation probabilities (Figure 3), in the same way as for normal incidence and $0.25 \text{ eV} < E_i < 0.75 \text{ eV}$.

RPBE-AIMD indirect dissociation probabilities and trapping probabilities are larger than the corresponding GLO probabilities. Curiously, when considering the RPBE functional, we observe that at the lowest collision energy simulated for normal incidence ($E_i = 0.9$ eV) and at the highest collision energy simulated for $\Theta_i = 60^\circ$ ($E_i \approx 2.3$ eV), AIMD yields trapping mediated reaction

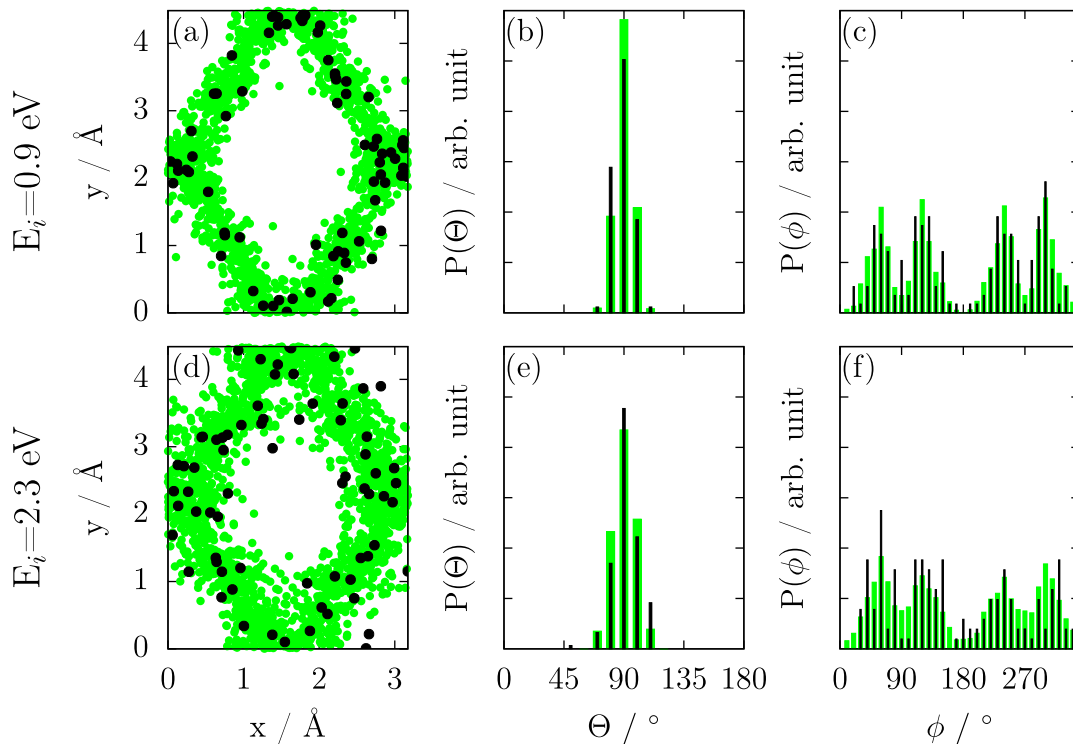


FIG. 5. Distributions at the moment of dissociation (defined to occur when r equals twice the N_2 equilibrium bond length with positive radial velocity) for two representative initial collision energies ($E_i = 0.9$ eV top and $E_i = 2.3$ eV bottom). The first, second and third columns present the X and Y positions of the center of mass of the molecules, θ distributions and ϕ distributions, respectively. PBE-AIMD data are plotted as large black symbols (for the X, Y positions) and as black bars (for the θ and ϕ distributions), while PW91-GLO data are plotted as small green symbols (for the X, Y positions) and as green bars (for the θ and ϕ distributions).

probabilities that are much higher than the static surface trapping-mediated dissociation probabilities, while for the same initial conditions the GLO and the static surface models return basically identical indirect dissociation probabilities. We have investigated whether the initial distortion of the lattice as included in AIMD could be a reason for this difference, considering that both models account for energy dissipation to phonons. In a similar (but extended) analysis as performed in Ref. 24, we have therefore separately investigated the effect of surface atom motion and lattice distortion considering $E_i = 2.287$ and $\Theta_i = 60^\circ$ as initial conditions. For this collision energy and incidence angle the relative (not absolute) difference between the static surface and the AIMD dissociation probabilities is the highest. In addition to AIMD calculations that include both surface atom motion and surface distortion, we have performed AIMD calculations (i) on an ideal frozen lattice, (ii) on a distorted frozen lattice, and (iii) on an (initially) ideal lattice, but allowing the surface atoms to move (i.e., simulating an initial surface temperature $T_S = 0$ K neglecting zero-point effects for the lattice). Results are shown in Table I. We observe that the dissociation probability computed with AIMD simulating an ideal frozen lattice is slightly larger than that computed using the RPBE-PES, the reason being small interpolation errors in the RPBE-PES as already noted in Ref. 47. More importantly, as also observed in Ref. 24 for another collision energy, incidence angle, and functional, allowing surface

atom motion seems to be the main responsible factor for the increase in reactivity. Lattice distortion seems not to play a role here: results obtained simulating an ideal frozen lattice agree within error bars with AIMD calculations simulating a frozen distorted lattice, while the reaction probabilities resulting from calculations including surface atom motion simulating either an initially distorted or an ideal surface are considerably larger than the reaction probabilities obtained with frozen surface calculations, and in agreement with each other (at least in the upper bounds to dissociation probabilities). Accounting for surface relaxation effects and/or for energy transfer to the surface phonons seem therefore to be the elements in AIMD that cause the increase in reactivity with respect to the static surface model, regardless of whether (static) surface distortion effects are modeled or not. The main cause of the increase of reactivity observed when the surface atoms are allowed to move is the increase of the trapping mediated reactivity.

B. Dissociation dynamics

In this section, we compare AIMD and GLO for a few detailed features of the dissociation dynamics. We start by comparing AIMD and GLO for the position and orientation of the molecules at the moment of dissociation. Figure 5 illustrates the position of the center of mass of the dissociating molecules above the surface (X, Y), and the distributions of the polar angle θ and of the azimuthal angle ϕ that describe

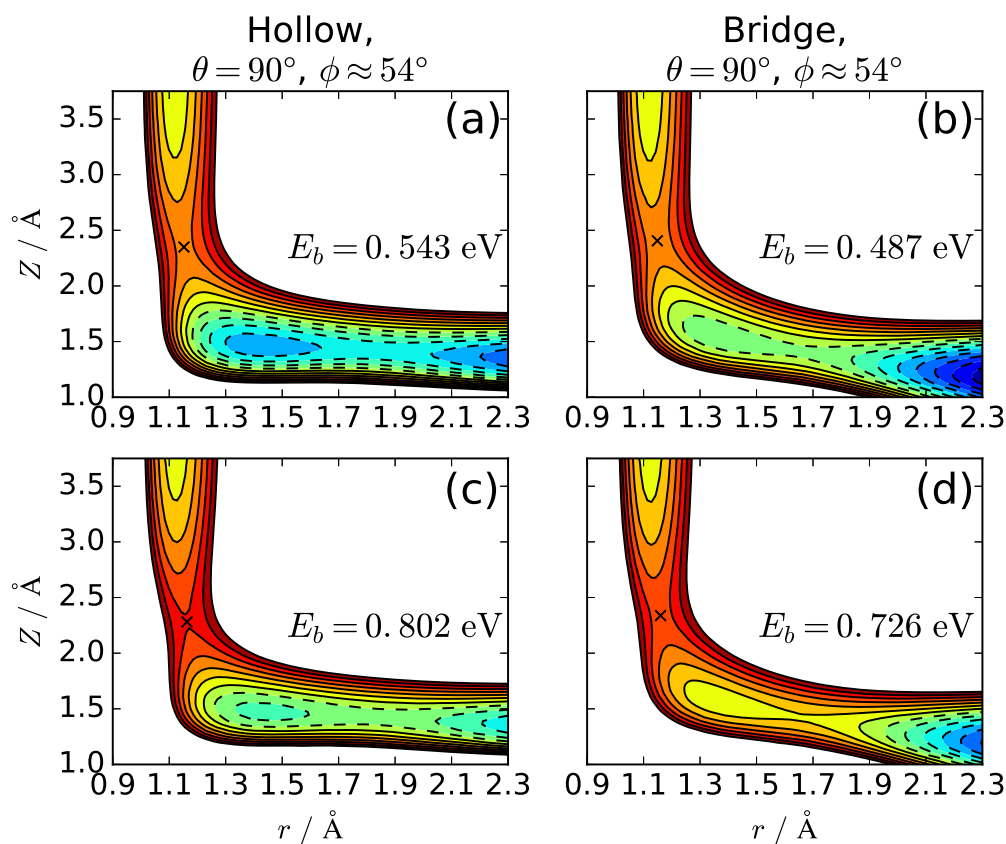


FIG. 6. Interaction energy as a function of r and Z for two configurations of N_2 , hollow (panels (a) and (c)) and bridge (panels (b) and (d)). Panels (a) and (b) are for PBE and (c) and (d) are for RPBE. A black \times indicates the position of the saddle point in the entrance channel. Interaction energies have been evaluated on a dense grid and spline interpolated for illustration purposes. Contour lines separate 0.2 eV energy intervals up to a maximum of 1.2 eV. Dashed lines identify negative energy values.

the orientation of the molecular bond. We have chosen two representative collision energies for normal incidence and a representative functional, but similar plots are observed for any combination of collision energy and functional, and also for $\Theta_i = 60^\circ$. For both theoretical models and in agreement with the static surface results of Refs. 38, 41, and 47, the dissociation occurs in the proximity of the hollow or bridge site (Figures 5(a) and 5(d)), with the bond oriented parallel to the surface, i.e., with $\theta = 90^\circ$ (Figures 5(b) and 5(e)). For both GLO and AIMD, the two N atoms are pointing towards the neighboring bridge sites (if the center of mass is above the hollow site) or towards the neighboring hollow sites (if the center of mass is above the bridge site). For the W(110) surface, these orientations correspond to the ϕ angles 54° and 126° (and equivalently 306° and 234°) in our reference frame, and ϕ distributions at the instant of dissociation are quite peaked around these values (see Figures 5(c) and 5(f)). The fact that very similar distributions were also obtained within the static surface approximation^{38,41,47} suggests that surface motion and surface temperature effects do not significantly affect the position and the orientation at which the molecules dissociate, and confirms the accuracy of the interpolation of the PESs used in the GLO and static surface calculations.

We now go on to show that AIMD and GLO not only predict similar distributions at the moment of the dissociation, but they also predict similar dynamics for specific sets of initial conditions. We start by considering the PBE-AIMD calculations at $E_i = 0.9$ eV and $\Theta_i = 60^\circ$. The barrier heights to dissociate above the hollow site and the bridge site with $\theta = 90^\circ$ are 0.54 and 0.49 eV, respectively, as extracted from two dimensional energy diagrams calculated with the computational setup employed in the AIMD calculations and assuming a frozen ideal surface (Figures 6(a) and 6(b)). Considering that only one fourth of the initial collision energy is directed along Z for $\Theta_i = 60^\circ$, at $E_i = 0.9$ eV the molecules oriented with the bond parallel to the surface cannot dissociate following the path of Figures 6(a) and 6(b), while they can, for instance, at $E_i = 2.287$ eV. Therefore, the molecules that go on to react at $E_i = 0.9$ eV are steered towards a particular orientation such that when they first reach $Z = 2.5$ Å, the θ distribution is quite peaked away from $\theta = 90^\circ$ around $\theta = 45^\circ$ (and the symmetry equivalent $\theta = 135^\circ$), as shown in Figure 7. This suggests that at this incidence angle and collision energy a preferred path exists for the molecules to approach the surface and that it involves the (re)orientation of the molecules to $\theta = 45^\circ$ (or $\theta = 135^\circ$). The center of mass

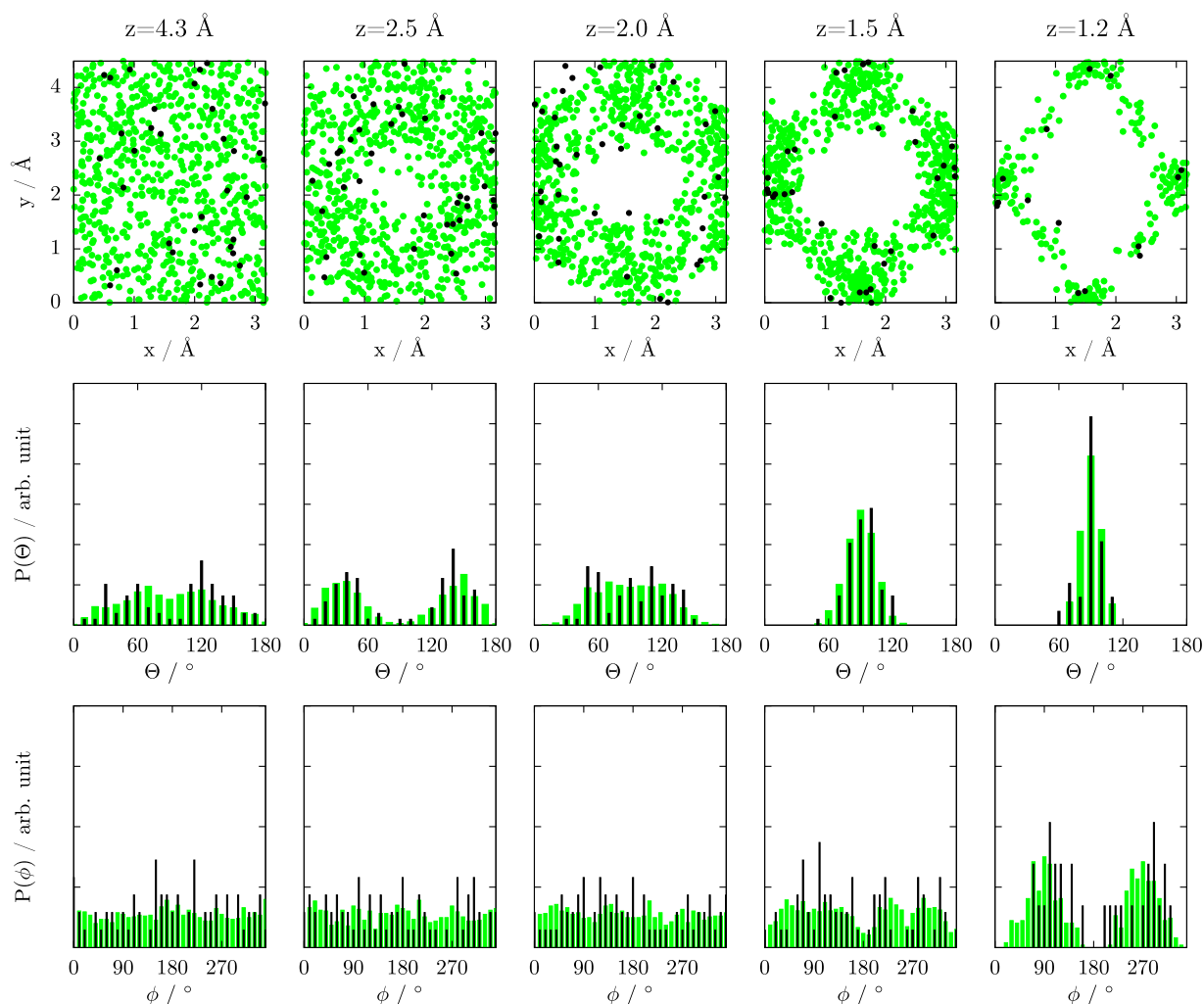


FIG. 7. Distributions evaluated for the reacting N_2 molecules when they first reach a specific Z value for $E_i = 0.9$ eV and $\Theta_i = 60^\circ$. The first, second, and third rows include the X and Y positions of the center of mass of the molecules, θ distributions, and ϕ distributions, respectively. Symbols and coloring as in Figure 5.

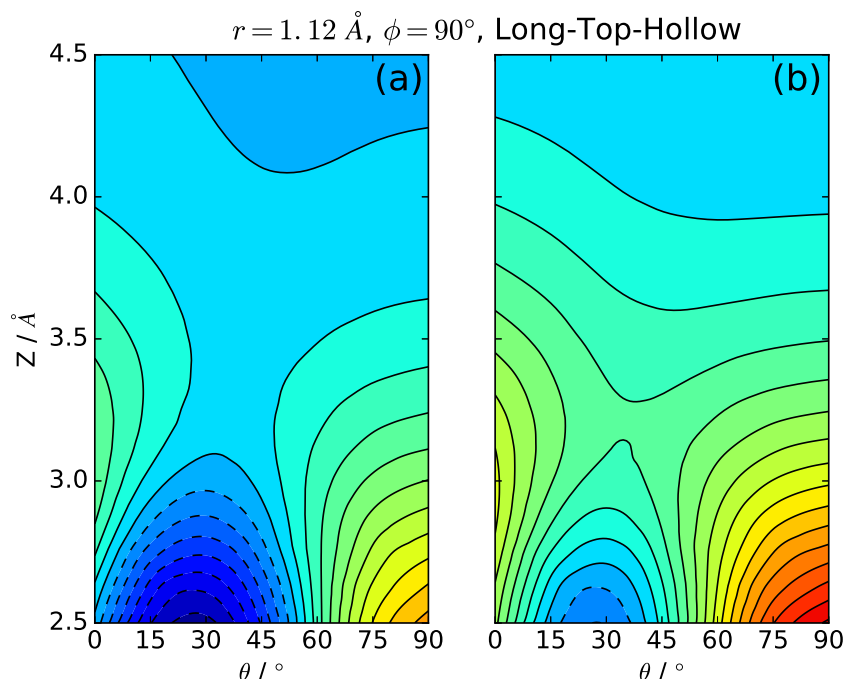


FIG. 8. Interaction energy as a function of θ and Z for N_2 above the long-top-hollow site. Panel (a) is for PBE and panel (b) is for RPBE. Interaction energies have been evaluated on a dense grid and spline interpolated for illustration purposes. Contour lines separate 50 meV energy intervals and dashed lines identify negative energy values.

position of the molecules when they first reach $Z = 2.5$ Å, also illustrated in Figure 7, is quite scattered across the surface unit cell, therefore, this path does not seem to be specific of a particular impact site. One of the impact sites where a tilted orientation is preferred over $\theta = 0^\circ$ and $\theta = 90^\circ$, is, for instance, the so-called long top-hollow site. This is clearly visible in Figure 8, where (θ, Z) two-dimensional energy diagrams illustrate that for $Z = 2.5$ Å the minimum of energy occurs for $\theta \approx 30^\circ$, for both PBE and RPBE.

When considering the PBE (PW91) functional, this connection of the reactivity to the evolving orientation of the molecule is not observed for $E_i = 2.287$ eV, $\Theta_i = 60^\circ$ and for $E_i = 0.9$ eV, $\Theta_i = 0^\circ$, as shown in Figure 9, presumably because for these combinations of collision energy and incidence angle the molecules have enough translational energy in Z to approach the surface and react with $\theta = 90^\circ$ following other paths, like the ones in Figures 6(a) and 6(b), and a θ distribution much closer to the initial $\sin \theta$ distribution is observed at $Z = 2.5$ Å for these initial conditions.

The same evolution of the orientation of the dissociating molecules as seen in AIMD is observed in the GLO dynamics, as shown, for instance, in Figure 7: At $E_i = 0.9$ eV and $\Theta_i = 60^\circ$ the θ distribution computed at $Z = 2.5$ Å is clearly peaked around $\theta = 45^\circ$ and $\theta = 135^\circ$. As also observed in the PBE-AIMD calculations, in GLO dynamics this reorientation mechanism is not followed at the same collision energy for normal incidence (Figure 9).

The dynamics just described is not specific of the PBE (PW91) calculations, it also extends to the RPBE calculations. For RPBE, the barrier to dissociate above the hollow and bridge sites is about 0.2-0.3 eV higher than for PBE (see Figures 6(c) and 6(d)). Therefore, for $\Theta_i = 60^\circ$, N_2 molecules cannot dissociate on the surface following the minimum paths in Figures 6(c) and 6(d), even at the highest collision energy simulated ($E_i = 2.287$ eV). The θ distributions for the reacting molecules at this collision energy and incidence angle, as

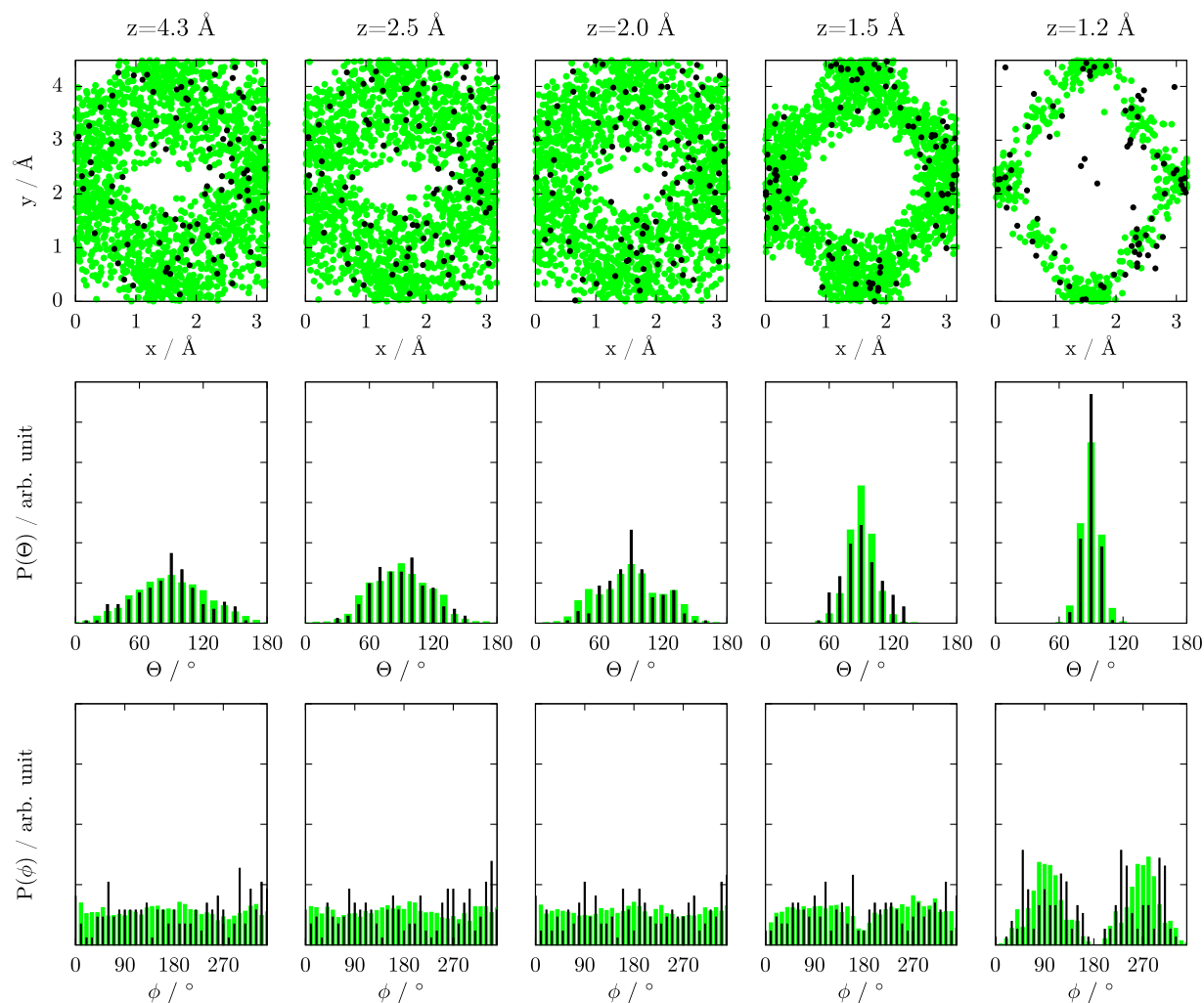
shown in Figure 10, are found to be similar to the ones computed with PBE at $E_i = 0.9$ eV and $\Theta_i = 60^\circ$ (Figure 7). Again, GLO calculations on the RPBE-PES predict similar distributions as RPBE-AIMD, with less noise thanks to the larger number of trajectories (and therefore better statistics) that can be computed with this method.

Once more, these findings are not specific to the AIMD and GLO model, but a similar dynamics is observed for the same initial conditions within static surface calculations,^{38,41,47} confirming again the accuracy of the interpolation procedure employed and the minor influence of surface motion and surface temperature effects on the dissociation dynamics for such initial conditions.

C. Energy transfer to the lattice for scattered N_2

Both the GLO model and the AIMD method allow the simulation of energy exchange between the molecular and the lattice degrees of freedom. In this section, we quantitatively compare the energy loss to the surface as predicted by the two theoretical models for the scattered trajectories, i.e., the trajectories in which the molecule is reflected back to the gas phase after the impact with the surface. In Figure 11 the average changes in total energy for N_2 , as obtained with AIMD and with the GLO model, are plotted as a function of the initial collision energy E_i . Note that we employ here a negative sign to indicate energy being transferred from the molecule to the surface. The energy transfer to the lattice ΔE as expected from the Baule model,^{6,7} according to which $\Delta E = \frac{4\mu}{(1+\mu)^2} E_i$, where μ is the ratio between the mass of the molecule and the mass of a surface atom, is also plotted in Figure 11.

Overall, AIMD and GLO predict similar average energy losses to surface phonons. This is particularly true for normal incidence, where the agreement between the two methods is very good, regardless of which functional is considered. For

FIG. 9. Same as Figure 7, but for $E_i = 0.9$ eV and $\Theta_i = 0^\circ$.

$\Theta_i = 60^\circ$, the agreement is less good, and the AIMD method predicts more energy transfer to the lattice than the GLO model at the highest collision energies simulated.

For both AIMD and GLO, larger energy losses are observed for normal incidence than for $\Theta_i = 60^\circ$. Two elements contribute to this. In the first place, the normal translational energy is more effective in helping the molecules to access the region of the potential close to the surface, where the molecules can become trapped and transfer energy to the lattice through multiple rebounds. From Figure 12, where we have plotted as a function of E_i the average number of rebounds that the molecules perform on the surface before being reflected, it is clearly visible that the average number of rebounds is generally larger for normal incidence than for $\Theta_i = 60^\circ$. This is also consistent with the larger trapping probabilities observed for normal incidence than for $\Theta_i = 60^\circ$ (Figure 4). Note that the agreement between the AIMD method and the GLO model in the average number of rebounds is good to very good. In the second place, the normal component of the translational energy is more efficiently transferred to the lattice degrees of freedom compared to its parallel components. In fact, at the highest collision energies, where the average number of rebounds is similar for the two incidence angles (Figure 12), we still observe a larger energy transfer at normal

incidence than for $\Theta_i = 60^\circ$. The fact that AIMD predicts larger energy transfer than GLO for $\Theta_i = 60^\circ$ (especially if the PBE/PW91 functional is considered) while similar energy transfer is observed at normal incidence, together with the average number of rebounds being very similar for the two techniques for both incidence angles, suggests that the GLO model somewhat underestimates the amount of energy being transferred to the surface from the parallel components of the collision energy.

Compared to the Baule model, AIMD and GLO predict significantly less energy transfer to the lattice, for both normal incidence and $\Theta_i = 60^\circ$. This is also consistent with the results of Pétuya *et al.*,¹⁷ who found the Baule model to significantly overestimate the energy transfer to the lattice as predicted by the GLO model for N₂ scattering from a different low-index tungsten surface (W(100)). In Figures 11(b) and 11(d) we also show the energy transfer to the surface as predicted by the Baule model assuming that only the normal component of the collision energy could be transferred to the lattice (i.e., $\Delta E = \frac{4\mu}{(1+\mu)^2} E_n$, with $E_n = E_i \cos^2 \Theta_i$). Under this assumption, the agreement between the GLO and the Baule model improves, in particular if the PW91 functional is employed and if the highest collision energies simulated are considered, while PBE-AIMD calculations predict more

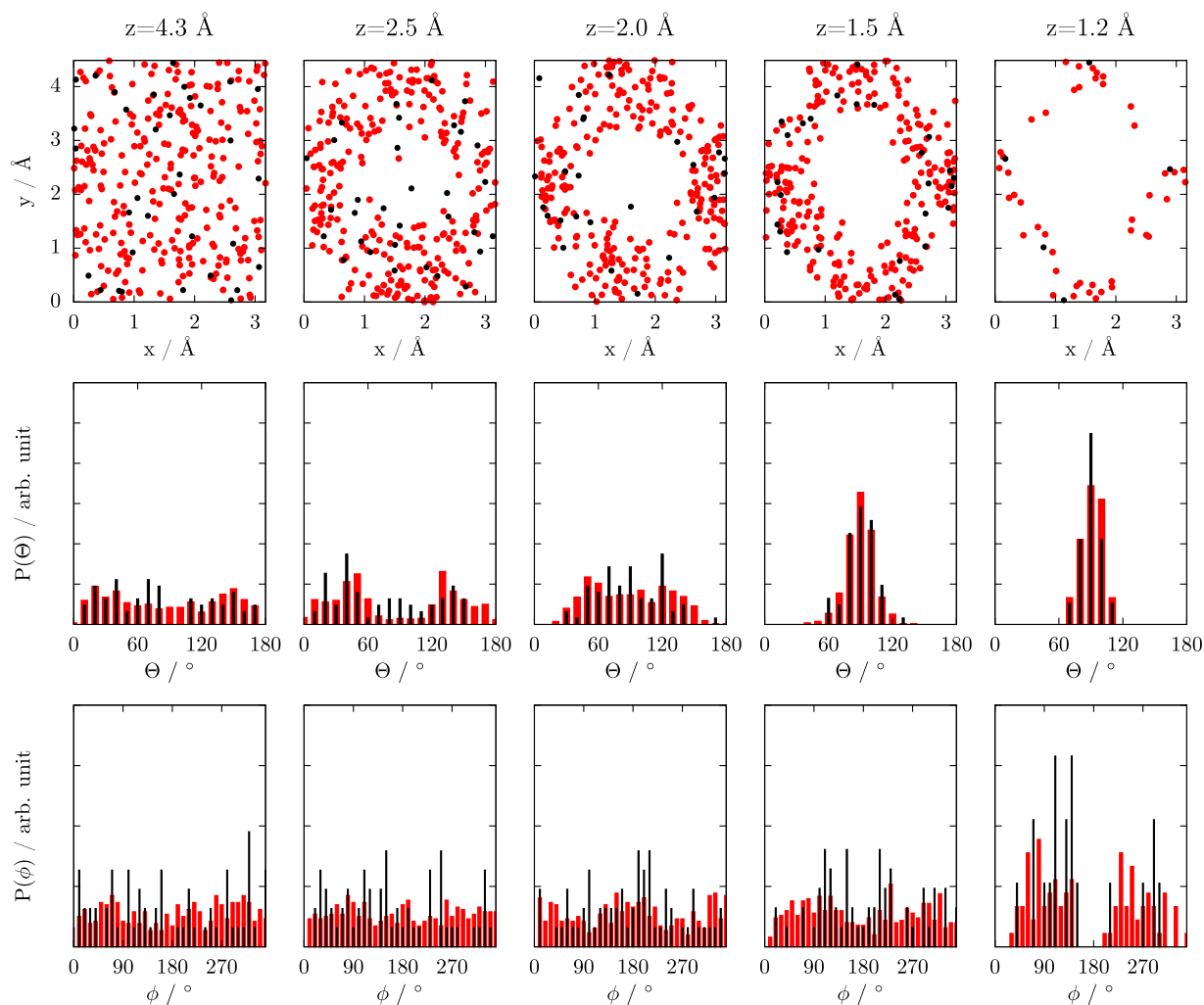


FIG. 10. Same as Figure 7, but for RPBE calculations, $E_i = 2.3$ eV and $\Theta_i = 60^\circ$ (red is used instead of green for the GLO data).

energy being transferred to the surface for the same values of E_i . Note, however, that the Baule model assumes the energy transferred to the surface to derive from a single binary collision between the molecule and a surface atom, while the average number of rebounds for the scattered N_2 molecules is somewhat larger (≈ 1.5 – 2) at the E_i considered here (Figure 12), for both AIMD and GLO.

For both normal incidence and $\Theta_i = 60^\circ$, the average energy losses are slightly larger for PBE (PW91) than for RPBE, both if the AIMD method and the GLO model is considered (Figure 11). This is consistent with the fact that the PBE (PW91) functional predicts considerably deeper molecular adsorption wells compared to the RPBE functional (the difference can be as large as 0.45 eV²⁴). Therefore, a larger increase in collision energy is expected for the molecules approaching the surface when the former functional is employed, resulting in a larger energy transfer. Note that this is the reasoning behind the so-called modified Baule model, in which E_i is replaced by $E_i + V$ in the traditional Baule model expression,^{6,7} V being the depth of the potential well over which the molecules fly before the impact with the surface. Furthermore, we note that for $\Theta_i = 60^\circ$ and for most of the collision energies considered, the PBE (PW91) functional

predicts a somewhat larger average number of rebounds for the scattered molecules than the RPBE functional (Figure 12).

The good agreement found between AIMD and GLO is not limited to the average energy transfer but extends to the corresponding distributions, as shown in Figure 13 where the distributions of the total energy change for the scattered N_2 molecules are plotted for the various incidence energies and angles and functionals. Distributions are generally more peaked and shifted to lower (absolute) energies for $\Theta_i = 60^\circ$, consistently with the lower number of rebounds that the molecules experience at high incidence angles (Figure 12). Distributions also become broader with increasing collision energy. The agreement between AIMD and GLO is poorest for $\Theta_i = 60^\circ$ at the highest collision energies simulated, where AIMD predicts broader distributions, consistently with the larger average energy loss predicted by this method.

D. Comparison to experiments

In Figure 14 we compare AIMD and GLO dissociation probabilities to available experimental data. Two experimental sets of data are available for normal incidence,^{29,32} while only one set of sticking probabilities has been reported

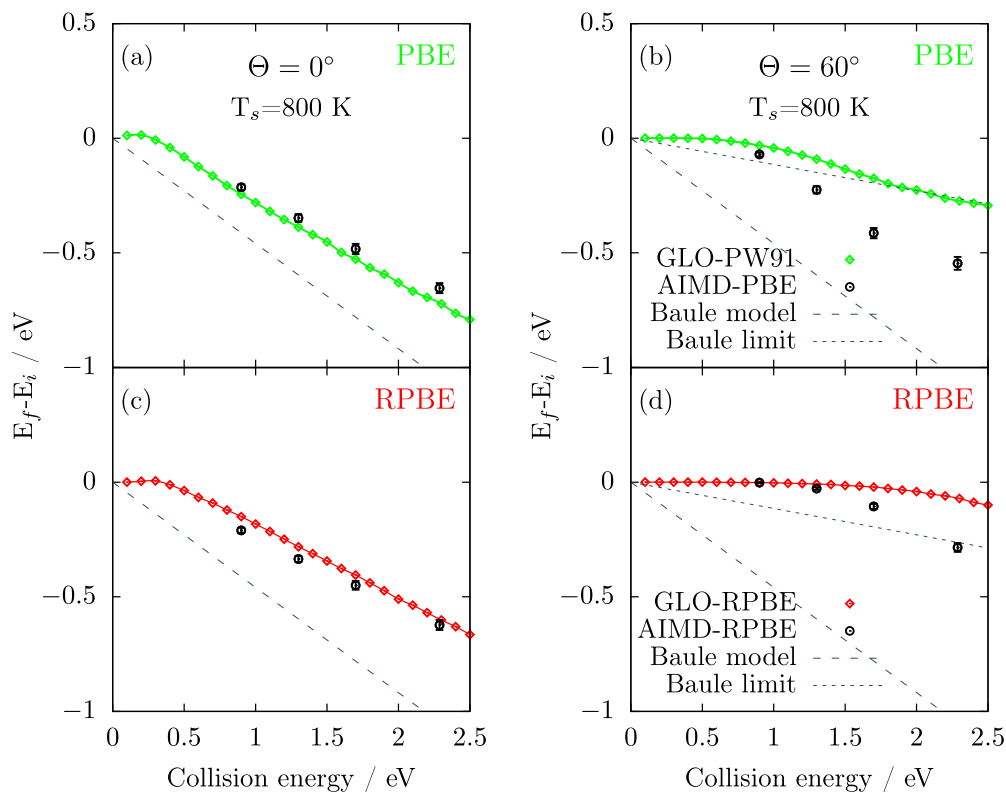


FIG. 11. Change in the total energy for the scattered N_2 molecules as a function of the incidence energy (AIMD results as circles, GLO results as diamonds). (a) PBE (PW91 for GLO) and normal incidence, (b) PBE (PW91 for GLO) and 60° incidence, (c) RPBE and normal incidence, and (d) RPBE and 60° incidence. The dashed lines represent the change in energy as predicted by the Baule model, and the dotted lines the change in energy as predicted by the Baule model assuming that only the normal component of the incidence energy is transferable to the lattice.

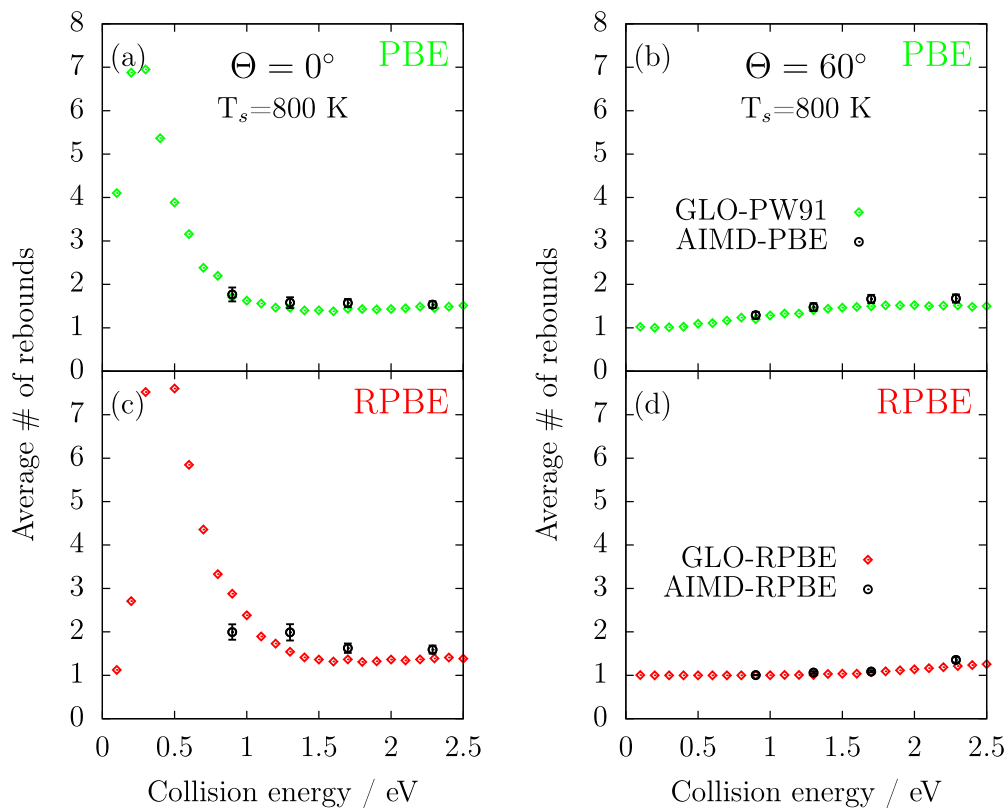


FIG. 12. Average number of rebounds for the scattered N_2 molecules (symbols and coloring as in Figure 11).

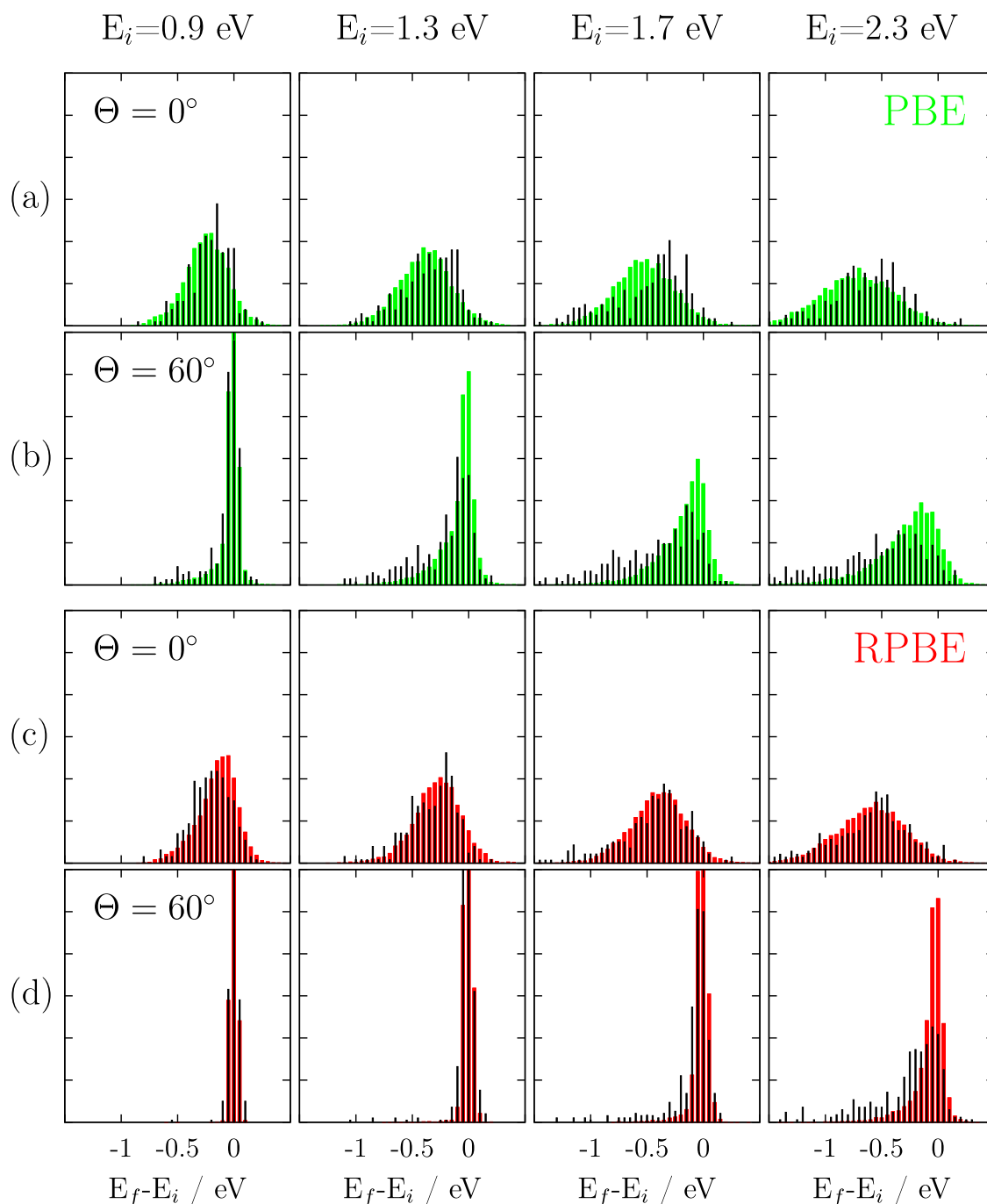


FIG. 13. Distributions of the total energy change for the scattered N_2 molecules. AIMD results are plotted as black bars, GLO results as green/red bars. Panels (a) are for PBE (PW91 for GLO) and normal incidence, (b) for PBE (PW91 for GLO) and 60° incidence, (c) for RPBE and normal incidence, and (d) for RPBE and 60° incidence.

for $\Theta_i = 60^\circ$.²⁹ As already concluded in Ref. 24 for normal incidence, AIMD is not able to accurately describe either of the two experimental sets of data over a wide range of collision energies, whether the PBE or the RPBE functional is employed. Also for $\Theta_i = 60^\circ$, the agreement with experimental data is limited: PBE-AIMD reaction probabilities are considerably too high compared to the experimental probabilities, while RPBE-AIMD reaction probabilities are too low. Similarly, the GLO model overestimates the experimental sticking probabilities, especially at the lowest collision energies at normal incidence if the PW91-PES is employed, while it predicts too low

dissociation probabilities for $\Theta_i = 60^\circ$ if the RPBE-PES is employed.

Overall, for the two sets of functionals studied (PW91/PBE and RPBE) modeling surface temperature effects does not systematically improve the agreement with experimental data compared to static surface simulations. If the PBE (or PW91) functional is considered, surface motion effects as modeled either with AIMD or with the GLO model worsen the agreement for both normal incidence and $\Theta_i = 60^\circ$. No considerable improvement with respect to static surface data is observed if the GLO model is employed in combination with the RPBE-PES. On the other hand, surface motion

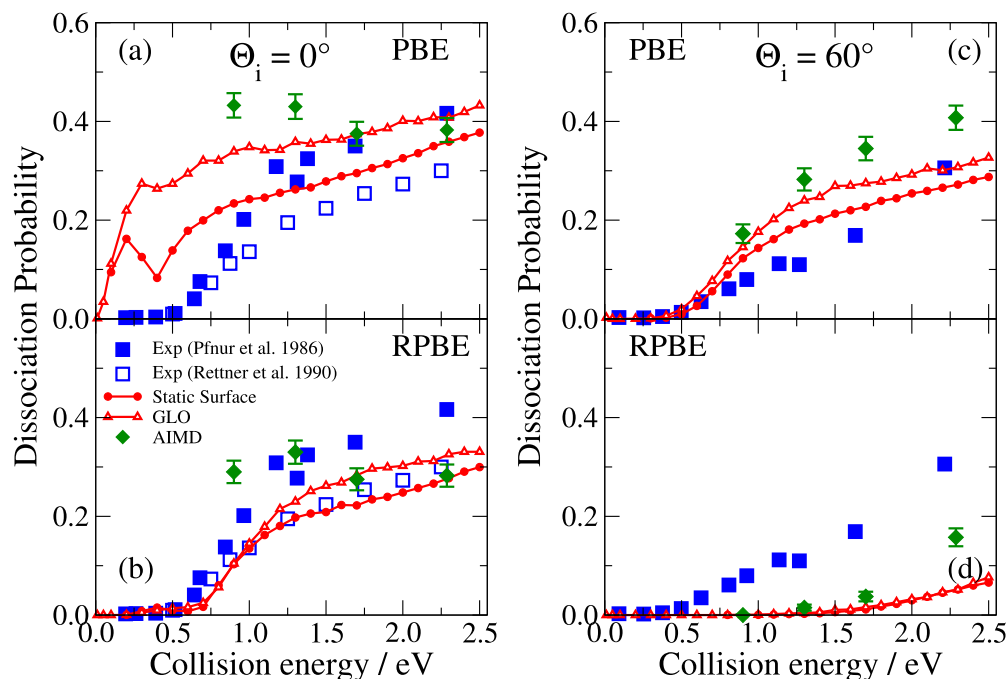


FIG. 14. Dissociation probabilities as a function of the collision energy: two sets of experimental data (solid and empty blue squares),^{29,32} static-surface calculations (red circles), GLO (red triangles) and AIMD (green diamonds). Panels (a) and (b) are for normal incidence, panels (c) and (d) are for $\Theta_i = 60^\circ$. Panels (a) and (c) present PBE-AIMD results and PW91 GLO and static surface results, and panels (b) and (d) present results obtained with RPBE.

effects as modeled with the AIMD method slightly improve the agreement between theory and experiment for $\Theta_i = 60^\circ$ (especially at the highest collision energy simulated), while they worsen such agreement at normal incidence for the lowest collision energy simulated.

IV. SUMMARY AND CONCLUSIONS

Summarizing, we have performed a critical comparison of the AIMD method and the GLO model, investigating their ability to describe the dissociation of N_2 on W(110). The strong effect that surface motion effects have on the dissociation probability has been demonstrated earlier²⁴ and further confirmed here.

Despite the simplicity of the GLO model, we have found qualitative agreement with the AIMD dissociation probabilities at normal incidence and at $\Theta_i = 60^\circ$, both if the PBE or the RPBE functional is considered. Most importantly, the comparison with static surface dissociation probabilities reveals that the AIMD method and the GLO model agree on the effect of surface motion and surface temperature effects on the dissociation probability for the considered molecule-surface system. Both methods, in fact, suggest an increased reactivity due to a larger trapping-mediated dissociation probability. Good agreement between AIMD and GLO is observed in estimating the energy transferred to the surface for the molecules that are scattered back to the gas phase. Furthermore, the two models agree in predicting features of the dissociation dynamics, such as the evolution of the θ distribution for the molecules dissociating under specific conditions of incidence angle and collision energy.

As already anticipated in Ref. 24, where only normal incidence conditions were investigated, the AIMD method

fails at describing available experimental dissociation probabilities if the PBE or the RPBE functional is employed. Similarly, the PW91-GLO calculations return too large dissociation probabilities, especially at normal incidence and at the lowest collision energies, while RPBE-GLO dissociation probabilities are systematically too low for $\Theta_i = 60^\circ$. The limited accuracy of the density functional remains a potential obstacle on the way towards an accurate description of the dissociation of N_2 on tungsten surfaces.

SUPPLEMENTARY MATERIAL

See [supplementary material](#) for the GLO results obtained using different values of the parameters describing the surface and ghost oscillators.

ACKNOWLEDGMENTS

The Leiden group thanks the Nederlandse Organisatie voor Wetenschappelijk Onderzoek (Netherlands Organisation for Scientific Research, NWO) and the European Research Council for supporting this research through a TOP grant and a ERC-2013 advanced grant (Grant No. 338580), respectively. NWO Exacte Wetenschappen, EW (NWO Physical Sciences Division) is acknowledged for granting access to the Lisa and Cartesius supercomputers. O.G., R.D.M., and M.A. acknowledge financial support by the Basque Departamento de Educación, Universidades e Investigación, the University of the Basque Country UPV/EHU (Grant No. IT-756-13) and the Spanish Ministerio de Economía y Competitividad (Grant No. FIS2013-48286-C2-2-P). O.G. acknowledges the IDEX Bordeaux (No. ANR-10-IDEX-03-02) and Euskampus for fundings. Computational resources for the GLO calculations were provided by the DIPC computing center.

- ¹G. J. Kroes, *J. Phys. Chem. Lett.* **6**, 4106 (2015).
- ²A. C. Luntz and J. Harris, *Surf. Sci.* **258**, 397 (1991).
- ³S. Nave and B. Jackson, *Phys. Rev. Lett.* **98**, 173003 (2007).
- ⁴G. Henkelman and H. Jónsson, *Phys. Rev. Lett.* **86**, 664 (2001).
- ⁵M. Bonfanti, C. Díaz, M. F. Somers, and G. J. Kroes, *Phys. Chem. Chem. Phys.* **13**, 4552 (2011).
- ⁶B. Baule, *Ann. Phys.* **44**, 145 (1914).
- ⁷A. Gross, *Theoretical Surface Science* (Springer, Berlin, 2003).
- ⁸D. Novko, M. Blanco-Rey, J. I. Juaristi, and M. Alducin, *Phys. Rev. B* **92**, 201411 (2015).
- ⁹S. A. Adelman and J. D. Doll, *J. Chem. Phys.* **64**, 2375 (1976).
- ¹⁰J. C. Tully, *J. Chem. Phys.* **73**, 1975 (1980).
- ¹¹J. C. Polanyi and R. J. Wolf, *J. Chem. Phys.* **82**, 1555 (1985).
- ¹²H. F. Busnengo, W. Dong, and A. Salin, *Phys. Rev. Lett.* **93**, 236103 (2004).
- ¹³H. F. Busnengo, M. A. Di Césare, W. Dong, and A. Salin, *Phys. Rev. B* **72**, 125411 (2005).
- ¹⁴M. Hand and J. Harris, *J. Chem. Phys.* **92**, 7610 (1990).
- ¹⁵L. Martin-Gondre, M. Alducin, G. A. Bocan, R. Díez Muiño, and J. I. Juaristi, *Phys. Rev. Lett.* **108**, 096101 (2012).
- ¹⁶M. Blanco-Rey, E. Díaz, G. A. Bocan, R. Díez Muiño, M. Alducin, and J. I. Juaristi, *J. Phys. Chem. Lett.* **4**, 3704 (2013).
- ¹⁷R. Pétuya, P. A. Plötz, C. Crespos, and P. Larregaray, *J. Phys. Chem. C* **118**, 21904 (2014).
- ¹⁸I. Goikoetxea, J. Meyer, J. I. Juaristi, M. Alducin, and K. Reuter, *Phys. Rev. Lett.* **112**, 156101 (2014).
- ¹⁹V. J. Bukas, S. Mitra, J. Meyer, and K. Reuter, *J. Chem. Phys.* **143**, 034705 (2015).
- ²⁰I. Lončarić, M. Alducin, P. Saalfrank, and J. I. Juaristi, *Phys. Rev. B* **93**, 014301 (2016).
- ²¹A. Groß and A. Dianat, *Phys. Rev. Lett.* **98**, 206107 (2007).
- ²²A. Groß, *Chem. Phys. Chem.* **11**, 1374 (2010).
- ²³F. Nattino, C. Díaz, B. Jackson, and G. J. Kroes, *Phys. Rev. Lett.* **108**, 236104 (2012).
- ²⁴F. Nattino, F. Costanzo, and G. J. Kroes, *J. Chem. Phys.* **142**, 104702 (2015).
- ²⁵G. Ertl, *Catal. Rev.: Sci. Eng.* **21**, 201 (1980).
- ²⁶S. P. Singh-Boparai, M. Bowker, and D. A. King, *Surf. Sci.* **53**, 55 (1975).
- ²⁷J. T. Yates, R. Klein, and T. E. Madey, *Surf. Sci.* **58**, 469 (1976).
- ²⁸R. C. Cosser, S. R. Bare, S. M. Francis, and D. A. King, *Vacuum* **31**, 503 (1981).
- ²⁹H. E. Pfnür, C. T. Rettner, J. Lee, R. J. Madix, and D. J. Auerbach, *J. Chem. Phys.* **85**, 7452 (1986).
- ³⁰J. C. Lin, N. Shamir, Y. B. Zhao, and R. Gomer, *Surf. Sci.* **231**, 333 (1990).
- ³¹Q. J. Zhang, J. C. Lin, N. Shamir, and R. Gomer, *Surf. Sci.* **231**, 344 (1990).
- ³²C. T. Rettner, E. K. Schweizer, and H. Stein, *J. Chem. Phys.* **93**, 1442 (1990).
- ³³T. F. Hanisco and A. C. Kummel, *J. Vac. Sci. Technol., A* **11**, 1907 (1993).
- ³⁴A. Kara and A. E. DePristo, *J. Chem. Phys.* **88**, 2033 (1988).
- ³⁵G. Volpillac and A. Salin, *Surf. Sci.* **556**, 129 (2004).
- ³⁶C. Corriol and G. Darling, *Surf. Sci.* **557**, L156 (2004).
- ³⁷M. Alducin, R. Díez Muiño, H. F. Busnengo, and A. Salin, *Phys. Rev. Lett.* **97**, 056102 (2006).
- ³⁸M. Alducin, R. Díez Muiño, H. F. Busnengo, and A. Salin, *J. Chem. Phys.* **125**, 144705 (2006).
- ³⁹M. Alducin, R. Díez Muiño, H. F. Busnengo, and A. Salin, *Surf. Sci.* **601**, 3726 (2007).
- ⁴⁰J. I. Juaristi, M. Alducin, R. Díez Muiño, H. F. Busnengo, and A. Salin, *Phys. Rev. Lett.* **100**, 116102 (2008).
- ⁴¹G. A. Bocan, R. Díez Muiño, M. Alducin, H. F. Busnengo, and A. Salin, *J. Chem. Phys.* **128**, 154704 (2008).
- ⁴²A. C. Luntz, I. Makkonen, M. Persson, S. Holloway, D. M. Bird, and M. S. Miziański, *Phys. Rev. Lett.* **102**, 109601 (2009).
- ⁴³J. I. Juaristi, M. Alducin, R. Díez Muiño, H. F. Busnengo, and A. Salin, *Phys. Rev. Lett.* **102**, 109602 (2009).
- ⁴⁴I. Goikoetxea, J. I. Juaristi, M. Alducin, and R. Díez Muiño, *J. Phys.: Condens. Matter* **21**, 264007 (2009).
- ⁴⁵L. Martin-Gondre, C. Crespos, P. Larregaray, J. C. Rayez, B. van Ootegem, and D. Conte, *J. Chem. Phys.* **132**, 204501 (2010).
- ⁴⁶K. R. Geethalakshmi, J. I. Juaristi, R. Díez Muiño, and M. Alducin, *Phys. Chem. Chem. Phys.* **13**, 4357 (2011).
- ⁴⁷L. Martin-Gondre, J. I. Juaristi, M. Blanco-Rey, R. Díez Muiño, and M. Alducin, *J. Chem. Phys.* **142**, 074704 (2015).
- ⁴⁸D. Migliorini, F. Nattino, and G. J. Kroes, *J. Chem. Phys.* **144**, 084702 (2016).
- ⁴⁹J. P. Perdew, J. A. Chevary, S. H. Vosko, K. A. Jackson, M. R. Pederson, D. J. Singh, and C. Fiolhais, *Phys. Rev. B* **46**, 6671 (1992).
- ⁵⁰J. P. Perdew, J. A. Chevary, S. H. Vosko, K. A. Jackson, M. R. Pederson, D. J. Singh, and C. Fiolhais, *Phys. Rev. B* **48**, 4978 (1993).
- ⁵¹B. Hammer, L. B. Hansen, and J. K. Nørskov, *Phys. Rev. B* **59**, 7413 (1999).
- ⁵²J. P. Perdew, K. Burke, and M. Ernzerhof, *Phys. Rev. Lett.* **77**, 3865 (1996).
- ⁵³J. P. Perdew, K. Burke, and M. Ernzerhof, *Phys. Rev. Lett.* **78**, 1396 (1997).
- ⁵⁴M. Dion, H. Rydberg, E. Schröder, D. C. Langreth, and B. I. Lundqvist, *Phys. Rev. Lett.* **92**, 246401 (2004).
- ⁵⁵K. Lee, E. D. Murray, L. Kong, B. I. Lundqvist, and D. C. Langreth, *Phys. Rev. B* **82**, 081101 (2010).
- ⁵⁶J. Klimeš, D. R. Bowler, and A. Michaelides, *J. Phys.: Condens. Matter* **22**, 022201 (2010).
- ⁵⁷G. Kresse and J. Hafner, *Phys. Rev. B* **47**, 558 (1993).
- ⁵⁸G. Kresse and J. Hafner, *Phys. Rev. B* **49**, 14251 (1994).
- ⁵⁹G. Kresse and J. Furthmüller, *Comput. Mater. Sci.* **6**, 15 (1996).
- ⁶⁰G. Kresse and J. Furthmüller, *Phys. Rev. B* **54**, 11169 (1996).
- ⁶¹G. Kresse and D. Joubert, *Phys. Rev. B* **59**, 1758 (1999).
- ⁶²H. F. Busnengo, A. Salin, and W. Dong, *J. Chem. Phys.* **112**, 7641 (2000).
- ⁶³L. S. Dubrovinsky and S. K. Saxena, *Phys. Chem. Miner.* **24**, 547 (1997).
- ⁶⁴M. Balden, S. Lehwald, and H. Ibach, *Phys. Rev. B* **53**, 7479 (1996).
- ⁶⁵W. L. Hays, *Statistics* (Holt-Saunders, Tokyo, 1981).